Quaternary and Environmental Geosciences (2026) 17(1):58-73

Holocene coastal plain stratigraphic succession (Maracanã / Eastern Amazon, Brazil)

Sucessão estratigráfica de planície costeira holocênica (Maracanã / Amazônia Oriental, Brasil)

Maamar El-Robrini[ab]

[a]Faculdade de Oceanografia da Universidade Federal do Pará
[d]robrini@ufpa.br

Abstract

This article aims to identify the sedimentary infill (recent stratigraphy - 2 m) and the source of the sediments, through the analysis of clay minerals and heavy minerals, in the Maracanã Coastal Plain (Atlantic Coast of Pará), is narrow and develops along the margins of the Maracanã estuary, excavated into the coastal plateau (20-30 m high), which extends towards the Atlantic Ocean. The hydrological (water discharge of 450 m3/s) and hydrodynamic conditions (semi-diurnal macro tide: range of 5.4 m, and currents: up to 200 cm/s) make the Maracanã estuary one of the most important in the region. The results show that this coastal plain is filled with 3 sedimentary deposits: (i) Basal Unit S1 - tidal channel sands, mud, and estuarine sand, where clay minerals predominate (smectite/40-49%, kaolinite/30-38%, illite/20%), containing a large amount of zircon (56–35%) in the heavy mineral fraction; (ii) Regressive Unit S2 - fine and very fine sand (sandy plain/base) and, subsequently, organic mud (mangrove) and mud bar (top), with a predominance of smectite (42-47%) and a decrease in kaolinite (33-37%) and illite (15-24%). Staurolite (31–40%) is the predominant mineral in the heavy mineral fraction; (iii) Current Transgressive Unit S3 - current dune (top), beach ridge barrier and sandy-muddy bars (base), with clay minerals (smectite/44%, kaolinite/36%, illite/20%) and a higher occurrence of staurolite (29–34%) in the heavy mineral fraction. The clay minerals probably originate from the Amazon River (kaolinite). The heavy minerals indicate sources from the Barreiras Group and Post-Barreiras sediments, that occur along the entire Atlantic Coast of Pará and on the adjacent continental shelf. The beaches and dunes migrate over the mangroves due to aerodynamic and hydrodynamic forces and the rising sea level.

Keywords: Atlantic Coast of Pará; Stratigraphy; Heavy Minerals, Clay minerals.

Resumo

Este artigo tem como objetivo identificar o preenchimento sedimentar (estratigrafia recente – 2 m) e a origem dos sedimentos, através da análise de argilo-minerais e minerais pesados, na Planície Costeira do Maracanã (Costa Atlântica do Pará), sendo estreita e desenvolve-se às margens do estuário do rio Maracanã, escavado no planalto costeiro (20-30 m de altura), que se estende em direção ao Oceano Atlântico. As condições hidrológicas (vazão de 450 m³/s) e hidrodinâmicas (macro-maré semidiurna: amplitude de 5,4 m, e correntes: até 200 cm/s) tornam o estuário do rio Maracanã um dos mais importantes da região. Os resultados mostram que esta planície costeira é preenchida por 3 depósitos sedimentares: (i) Unidade Basal S1 - areias de canal de maré, lama e areia estuarina, onde predominam argilo-minerais (esmectita/40-49%, caulinita/30-38%, ilita/20%), contendo uma grande quantidade de zircão (56–35%) na fração de minerais pesados; (ii) Unidade Regressiva S2 - areia fina e muito fina (planície arenosa/base) e, subsequentemente, lama orgânica (mangue) e banco lamosos (topo), com predominância de esmectita (42-47%) e diminuição de caulinita (33-37%) e ilita (15-24%). A estaurolita (31–40%) é o mineral predominante na fração de minerais pesados; (iii) Unidade transgressiva atual S3 - duna atual (topo), barreira de crista de praia e bancos arenosos-lamosos (base), com argilo-minerais (esmectita/44%, caulinita/36%, ilita/20%) e maior ocorrência de estaurolita (29–34%) na fração de minerais pesados. Os argilo-minerais provavelmente têm origem no rio Amazonas (caulinita). Os minerais pesados indicam fontes provenientes dos sedimentos do Grupo de Barreiras e Pós-Barreiras, que ocorrem ao longo da Costa Atlântica do Pará e na plataforma continental adjacente. As praias e dunas migram sobre os manguezais devido às forças aerodinâmicas e hidrodinâmicas e ao aumento do nível do mar.

Palavras-chave: Costa Atlântica do Pará; Estratigrafia; Minerais pesados; Argilo-minerais.

1. Introduction

Coastal geomorphology and stratigraphic succession of geoarchives record past changes and fluctuations of coastal environments (May et al. 2013), and/or weather files (Humphries 2021). In addition, these geoarchives have the potential to store traces of past extreme events such as earthquakes and tsunamis, severe storms, and major inland coastal flooding. Due

https://doi.org/10.5380/qeg.v17i1.102013

to the same authors, by studying their sedimentological and ecological characteristics and their chronology, coastal changes throughout time can be reconstructed. Sediments that accumulate slowly in restricted areas such as swamps, lakes, lagoons preserve a variety of chemical signals that reflect the physical, chemical and biological characteristics of the environment, and analysis of the cores recovered from these environments can therefore provide a record of previous geological changes (Fritz 2008).

An estuary is a coastal environment with limited connection to the adjacent ocean, remains open at least intermittently, and can be subdivided into three zones: (1) river tidal zone (RTZ): river sector with salinity less than 1, but still subject to tides; (2) Mixing zone (MZ); (3) Coastal zone (Miranda et al. 2012). Due to Baum et al. (2024), estuaries are marine-flooded topographic depressions that receive sediment from both marine and fluvial sources. However, the amazon estuaries are well individuals and strongly influenced by the equatorial climate and meteorological processes (rain and drought periods, extreme events, winds), oceanographic (macrotide, waves), hydrological (water and solid discharges). Due to Röber & Rudolphi (2004) and IPCC (2022), sea level (SL) oscillations exert an important mechanism in the geological evolution of coastal areas, as any variation (in time and space) in the SL will reflect changes in the geomorphological arrangement of estuarine depositional systems. Tanabe et al. (2022) argue that the evolution of modern coastal depositional systems is governed primarily by Holocene SL oscillations. The sedimentation study in the estuarine areas is very important for understanding the environmental impacts, the coastal management, and the geological systems, to contribute in the model buildings for interpreting these systems. The Amazonian coastal zone has been evolving since the end of the last glacial period (Wisconsin), with the rise in SL to the current configuration in the form of indented coastline, characterized by a submergence coastline.

The Atlantic Coast of Pará with 600 km extension and NE - SW orientation is related to transgressive events occurring during the Holocene period (Cohen et al. 2020, Cohen et al. 2021). The Maracanã Coastal Plain (MCP)(Fig. 1) is part of this coast, which is influenced by macro-tide (5,4 m)(DHN 2026, El Robrini et al. 2018a), with extensive deposits of mud tidal flats, estuary, salt marshes, cheniers, dunes and beaches (Guerreiro et al. 2013, El Robrini et al. 2018a, Ranieri et al. 2022). The MCP is excavated in some geological layers: (i) marine limestones (Pirabas Formation/Lower Miocene) outcrop at the mouth of the Maracanã estuary (ii) conglomerates intercalated with sandy clay (Barreiras Group) form the cliffs bordering this estuary (iii) Post Barreiras sediments consist of sandy clay sediments and (iv) Recent - deposits of lower areas. The MCP is made up of (1) Coastal Plateau - cut by the Maracanã estuary, forming active cliffs at the mouth and low, inactive cliffs on the inside area; and (2) Coastal Plain - subdivided into (a) Muddy Plain (Mangrove) - consists of extensive deposits of fine sediments, rich in organic matter, occurring on the margins of the Maracanã estuary, forming low horizontal terraces, cut by tidal channels; (b) Estuarine Plain - formed by the ebb and flood channels of the Maracanã estuary and by the tidal channels, where point bars, mangrove islands and terraces occur; and (c) Sandy Plain - formed by cheniers, dunes and beaches.

Some studies have been conducted in the amazon coastal zone: stratigraphic studies and geological mapping (França et al. 2013, 2015, Guimarães et al. 2013a, 2013b, Buso et al. 2013a, 2013b, Cohen et al. 2020, 2021, Bezerra et al. 2014, 2015 and coastal dynamics (Silva & El Robrini, 2025, El Robrini et al. 2024, Herbert Junior & El Robrini, 2024, Menezes et al. 2024, El Robrini et al. 2018b, Guerreiro et al. 2016, Ranieri & El Robrini, 2015, 2016, 2020) has contributed to establish the morpho-stratigraphic successions, and the progressive knowledge in this region. Due to Castro et al. (2014), Cohen et al. (2021), Tanabi et al. (2022), the SL oscillations have an important role in the spatial and temporal arrangement of coastal sedimentary environments (Holocene). Most research has been conducted in the stretch between São João de Pirabas and Gurupí, where the coastal plateau is receding (inner part), with inactive cliffs and a well-developed coastal plain occupied by extensive mangrove plains. However, this article focuses on the narrow coastal plain embedded within the coastal plateau (stretch between São João de Pirabas and the Marajoará Golfão, 20-30 m high), which extends towards the Atlantic Ocean. In this latter stretch, there is no record of research, which motivated the development of this article aiming to identify the sedimentary infill (recent stratigraphy - 2 m) and the source of the sediments, through the analysis of clay minerals and heavy minerals in the Maracanã Coastal Plain.

2. Study area

The study area is located 164 km from Belém (capital of the state of Pará) and can be accessed via the BR316 highway to Santa Teresinha and then via the PA 127 highway to Maracanã (Fig. 1).

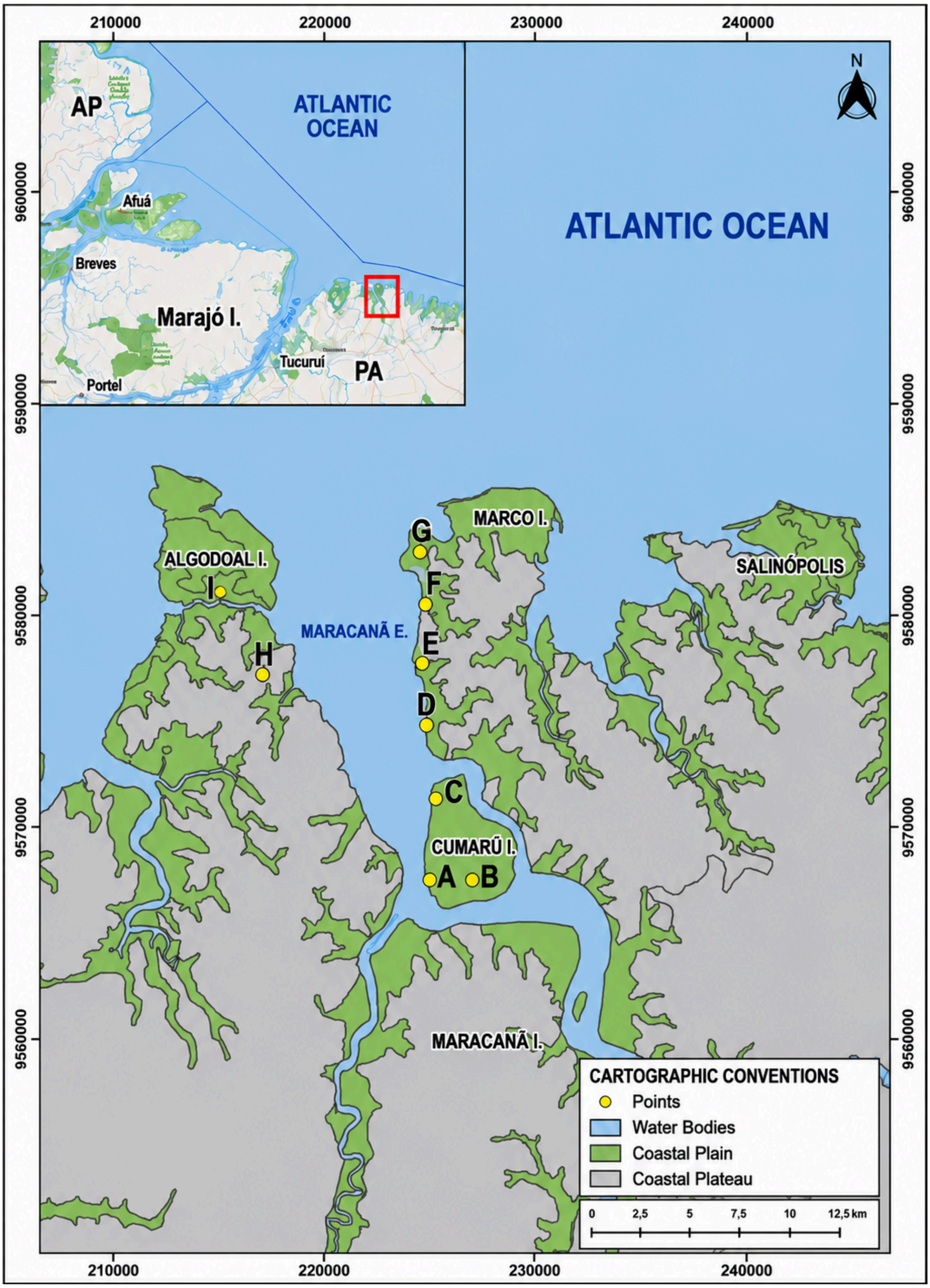

Figure 1: Location map and core samples (A. B. C. D. E. F. G. H) in the MCP (Atlantic Coast of Pará); I – Island; C - Channel.

2.1. Geologic Description

The lithostratigraphic units outcropping in the Maracanã estuary are: (i) Pirabas (ii) Barreiras Group (iii) Post-Barreiras (Rossetti et al. 2013) and (iv) recent sediments. Souza et al. (2014) show that the layers of Barreiras Group sediment are strongly moved by vertical to sub verticals faults, which extend up to a lesser degree, affecting Post-Barreiras and Quaternary sediments. The Maracanã estuary has a NW-SE orientation, where the left margin is occupied by high and active cliffs, while the right margin is lowered and covered by sandy banks. The NW-SE trend of normal faults could have developed within a transtensional regime related to the main event on the coast (Costa et al. 1996). According to the same authors, these faults correspond to the main components of the regional neotectonic framework; they favored the SL oscillations towards land, allowing the deposition of shallow marine sediments corresponding to the Pirabas/Barreiras Group Sediments.

2.2. Coastal Geomorphology of the Atlantic Coast of Pará

The Atlantic Coast of Pará extends for 600 km (between the mouth of the Amazon and Gurupi rivers), with strong structural control, following the orientations of normal NW-SE faults and NE-SW strike-slip faults (Cenozoic period) (Costa et al. 1996). This coast is subdivided into 2 sectors: (i) São João de Pirabas - Golfão Marajoará, where the coastal plateau (20-30 m high) is composed of Barreiras sediments. This plateau is cut by narrow estuaries, excavated into these sediments, and (ii) São João de Pirabas - Gurupí, which is a low coast, occupied by extensive mangrove plains, cut by estuaries carved mostly in Holocene deposits. The MCP is part of the first sector, where the macro-tidal reaches an range of 5,4 m (DHN, 2026) and the coastal plains are narrow and formed by estuarine floodplain (estuaries, tidal channels, point bars), muddy plains (mangroves) and sandy plains (beaches, dunes and paleodunes). The Maracanã estuary comprises the following parts: (1) upper - its source occurs in the Santa Maria do Pará river (South of Maracanã), with a depth of 4 m and a width of 30 to 60 m; (2) middle - depth of 4 to 8 m and width of 250 to 350 m; and (3) lower - depth of 4 to 17 m and width of 400 to 600 m. The seabed near the mouth of the Maracanã estuary is shallow and occupied by sandy tidal bars (Hylas, Beckle, Marapanim, and Maracanã banks) (NE-SW), following the same direction as the tidal currents. The seabed is predominantly sandy (fine and medium grain size) (El Robrini, 2012, El Robrini et al. 2018a). Algodoal and Marco islands are crowned by beaches (Fig. 1).

2.3.Weather Parameters

The climate characteristic of the Atlantic Coast of Pará is equatorial, with two periods: rainy (December to February) and dry (July to December), due to the seasonal displacement of the Inter-tropical Convergence Zone (ITCZ) over the region (Dubreuil et al. 2017). The average annual temperature is 27.2 °C and the average annual maximum temperature is 30.8 °C, with October to December being the hottest months, with an average of 31.6 °C (INMET, 2026). The average annual rainfall in this stretch of coastline is close to 1,800 mm, with a maximum of $>$ 2,700 mm. The effects of the ITCZ's position near the coast increase precipitation from summer to fall. In addition, the rainfall regime is influenced by El Niño and La Niña. Relative humidity is high and accompanies precipitation, with an annual average of 81 %. Normally, high values occur during the rainy season (January to June), with an average of 85 %, and during the dry season (July to December), with an average of 77 %, thus characterizing a humid region (INMET, 2026). Due to Germano et al. (2017), the wind direction diurnal cycle presents a Northeastern (NE), featuring the occurrence of the Sea Breeze (SB - most frequent from 1200 to 2100 UTC) on the same direction of the trade winds. The SB is much more pronounced, due to its proximity to the Atlantic Ocean, and the wind speed increases with the occurrence of the SB. The seasonal variation of the wind direction shows that the SB is more pronounced during the period of September-November (SON). It has a predominance of winds from E/NE during most of the year, due to its geographical position.

2.4. Oceanographic conditions

The Maracanã River has a hydrographic basin of 3,701 km² (ANA, 2025), with a water discharge of 450 m³/s (Mascarenhas, 2024). The tides are likely semi-diurnal, with an average amplitude of 5.4 m (spring tide) and 2.5 m (neap tide) (DHN, 2026) and the currents varying between 0.8 m/s and 2.1 m/s (Assireu et al. 2024). The harmonic analysis shows that M2 is the dominant constituent and the M2 and S2 components have amplitudes of 180 and 54 cm, respectively (Cavalcante et al. 2013). Sediment transport from the inner continental shelf (depth of 20 m) towards the coastal zone and the MCP occurs under the influence of interactions between waves and currents (Sawczyński & Kaczmarek, 2014). Salinity ranges from 7.6 to 10.12 (rainy season), but in the dry season, salinity tends to increase to 25.37 to 36 (El Robrini & Barbosa, 2012, El Robrini et al. 2018a). During the dry season (June-September), the ITCZ reaches its northernmost position and generates waves with an ENE flow direction (67.5°- 90°) and heights of 1.2 to 1.5 m and periods of 6 to 6.8 s (Guerreiro et al. 2020). When the wind blows from ENE (67.5°- 90°), during spring/autumn (transition from rainy/dry season), it generates waves with NE (45°- 67.5°) and ENE (67.5°- 90°) flow directions, with heights of 1.3 to 1.7 m and periods of 6.7 to 8.1 s. When the ITCZ reaches its southern position, it intensifies the NE trade winds, generating waves from the NNE (0°- 45°) during winter (rainy season/January-April), with a maximum height of 1.5 to 1.8 m and an average period of 8 s. However, in the Maracanã estuary, the waves have an average height of 0.53 m.

Several authors have estimated the solid discharge from the Amazon River exported to the Atlantic Ocean: 5×10^8 t/yr (Gibbs, 1967); 6×10^8 t/yr (Oltman, 1968); 11×10^8 t/yr to 13×10^8 t/yr (Meade et al. 1985); 550–1,500 Mt/yr (Gaillardet et al. 1997, Dunne et al. 1998, Guyot et al. 2005, Maurice-Bourgoin et al. 2007, Martinez et al. 2009); $5.50\text{-}10.30\times10^8$ t/yr (Filizola & Guyot, 2009); 9.5×10^8 t/yr (Pelletier, 2012); 4.06×10^8 t/yr (Fagundes et al. 2023); 37×10^8 t/yr (Hoch, 2014). The Amazon River flows into the Atlantic Ocean at 0° N, with an average volume of 209,000 m³/s into the ocean (Molinier et al. 1996), forming a freshwater plume that varies seasonally and spreads across the Tropical Atlantic. According to Diegues (1973), although the liquid transport of water from the Amazon

River was towards the NW, due to the North Coastal Current of Brazil, seasonal changes in wind direction result in the formation of a countercurrent near the coast, along the Atlantic Coast of Pará. According to the same author, fresh water (salinity < 10) extends 100-180 km from the coast, and brackish water (salinity between 11-35) covers most of the continental shelf west of the Amazon River during the rainy season. However, brackish waters extend to São Marcos Bay at the height of the rainy season (Diegues, 1973). During the dry season, fresh waters do not move much towards the ocean, nor do brackish waters move east of the Pará River along the Atlantic coast of Pará. This observation is corroborated by the work of Morozov et al. (2024), which determines that the existence of the plume intensifies the transport of currents to the Atlantic coast of Pará.

3. Materials and Methods

The analysis of sedimentological units was based on the interaction of surface and subsurface data, using cartography, facies analysis and correlation. The surface data was based on the study of outcrops (Landsat 7 ETM/4R5G3B composition, 2001) and the collection of mineralogical and textural samples. The sedimentary data was represented by columnar sedimentological sections (A, B, C, D, E, F, G, H), sampled by the vibracorer system that reached up to 2 m of penetration (Fig. 1). These sections were carried out on Cumaru Island (A, B, C), lowered right margin of the estuary (D, E, F, G) and Ponta of Algodoal Island (H), as the left margin is high, with the presence of cliffs, where the lower terrace is covered by thin layers of sediment (Fig. 1, Table 1). The core samples were cut into two longitudinal sections (one for sampling and the other for archiving). Descriptive analysis was performed on the samples, based on the methodology of Figueiredo (1990), followed by descriptive macroscopic analysis (model by Boyles et al. 1986), which highlighted color, lithological type, core length, sedimentary structures, grain size, and sedimentary facies succession. In the colors description (The Rock Color Chart, 2009), each color is represented by a standard code containing the characteristics of 3 parameters (10R 5/2): (i) 10R refers to hue, defined as a function of light wavelength (R - red, G - green, Y - yellow), (ii) 5/ corresponds to lightness, which is expressed as a function of the amount of black in relation to white, and (iii) 2 is the value referring to saturation, that is, the relative amount of pure color in relation to gray.

Grain size analysis was performed on the various units and samples (69) collected from the core intervals (colors) to quantify the different grain size fractions and obtain statistical parameters for the textural characterization of the sediments. The separation of the sand, silt, and clay fractions was performed by wet sieving, using a 0.063 mm sieve. The fraction that passed through this sieve is the silt/clay fraction. Thus, the separation of silt and clay was performed by centrifugation at 1,000 RPM (1,000 revolutions/minute) for 2 min, first precipitating the silt and leaving water+clay. The clay was separated from the water in the centrifuge at 2,000 RPM for 10 min. Oriented slides were prepared with a water/clay solution. The following pre-treatment was performed: the slides were: (1) dried at room temperature, (2) saturated with ethylene glycol, and (3) heated to 550 °C for 2 hours. After these processes, each slide was taken three times to the diffractometer in its normal form (air-dried), glycolated (addition of glycol for expansion), and heated (heated to 550 °C). Oriented slides were prepared using a water/clay solution for the analysis of clay minerals by X-ray diffraction (10 samples analyzed). After these processes, each blade was taken three times to the diffractometer, in its normal form (air-dried), glycolated (addition of glycol for expansion), and heated (heated to 550 °C). This procedure allowed the characterization and identification of clay minerals and other minerals (Albers et al. 2001) present in the samples through diffractograms, since each group behaves differently in each situation due to their specific structural loads. Subsequently, a semi-quantitative analysis of these clay minerals was performed using FullProf software to better characterize the clays and thus obtain the relative percentages. A Phillips PW 3020 diffractometer was used, connected to a PC installed in the X-ray Diffraction Laboratory, with CuKα radiation, 40 KV, 40 mA, automatic divergence slits 5 - 65° (2θ), speed of 0.04° (2θ/min), and counting time of 0.5 seconds.

For the sands, the total sample (150 g) was washed with distilled water and placed in an oven to dry at a temperature of 50 °C. The sand fraction was dry sieved through a set of sieves with mesh openings of 2.00 mm; 1.40; 1.00; 0.710; 0.500; 0.355; 0.250; 0.180; 0.125; 0.090, and 0.063 mm. The set of sieves with the sample was subjected to the action of an automatic agitator (ROTAP) for 10 min. Subsequently, the fractions retained in each sieve were weighed to obtain relative abundance percentages.

The heavy mineral separation technique was based on the use of bromoform ($CHBr_3$), in which the minerals, previously obtained by sieving (grain size fractions 0.250-0.125 mm and 0.125-0.062 mm)(27 samples analyzed each), were immersed in this liquid.

The identification of heavy minerals was done by making grain slides using Canada balsam (n=1.54) as the immersion liquid. The grains were then analyzed under a binocular magnifying glass at a maximum magnification of 40X for identification and counting, following the Line Counting method (Galehouse, 1971), in which the count is made along longitudinal lines, totaling 100 grains. The analysis made it possible to determine the assemblage and calculate ZTR indices (zircon, tourmaline, and rutile), which reflect the characteristics of the source rock (Adamu et al. 2020).

Table 1: Cores information, with Geographic Coordinates, Length (cm), Location in the Maracanã Coastal Plain.

Core Samples	Geographic Coordinates	Length (cm)	Location
A	47°28'10.45" W/ 0°44'23.06" S	150	Cumaru I.
B	47°26'59.53" W/ 0°44'40.78" S	150	Cumaru I.
C	47°27'44.89" W/ 0°42'11.16" S	130	Cumaru I.
D	47°28'28.16" W/ 0°39'24.62" S	130	lowered right margin
E	47°27'56.88" W/ 0°38'14.78" S	200	lowered right margin
F	47°28'46.42" W/ 0°36'51.88" S	120	lowered right margin
G	47°27'44.50" W/ 0°31'11.39" S	200	lowered right margin
H	47°32'29.36" W/ 0°37'48.11" S	150	Ponta of Algodoal I. - left margin

4. Results

4.1. Geomorphology of the Maracanã Coastal Plain

The Maracanã estuary is excavated in the Coastal Plateau, whose width varies from 400/600 m (mouth), 250/350 m (middle estuary) and 30/60 m (upper estuary) (Fig. 1). This estuary appears well developed in the inner and middle parts (Cumaru Island), and at the mouth of the Maracanã estuary (Algodoal and Marco Islands) (Fig. 2). On the Marco (West) and Algodoal (East) islands (Fig. 1) the main geomorphological units were identified: beaches, shoals, sandbanks, dunes, paleodunes, swamps and beach plains crests.

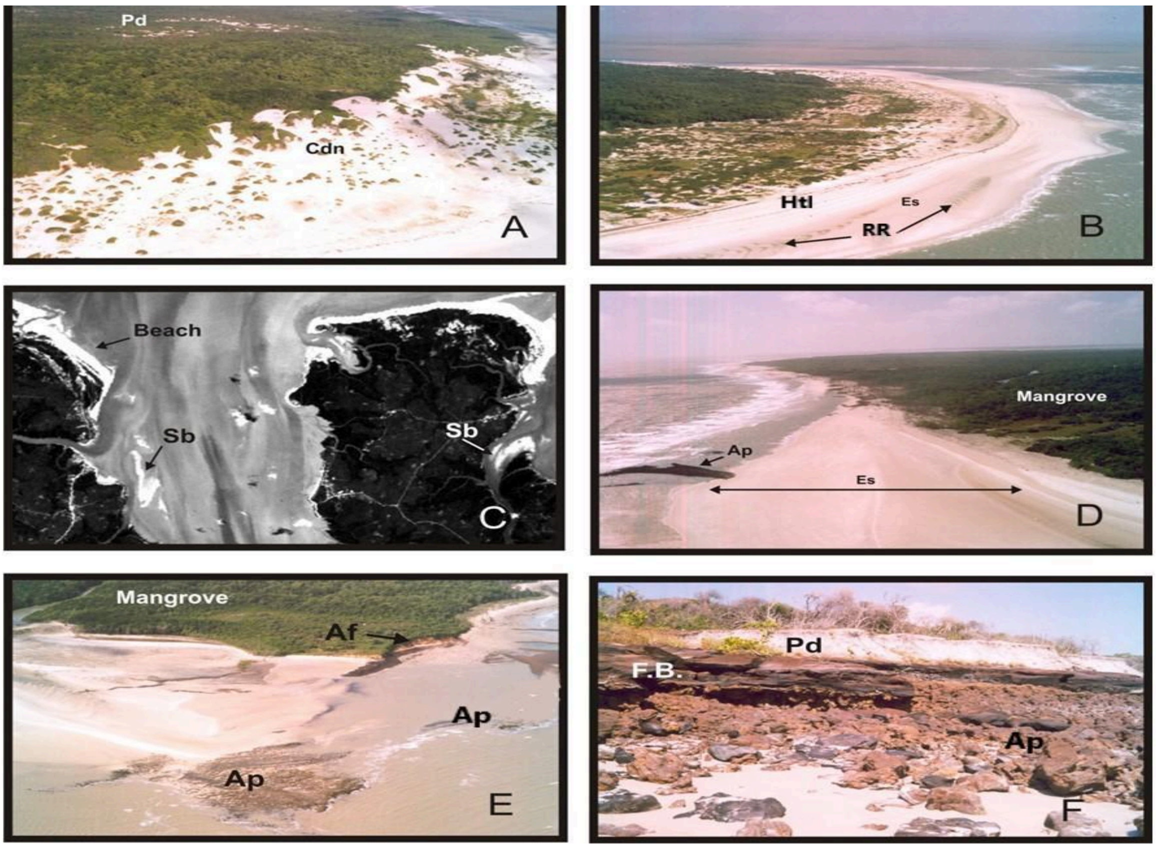

Figure 2: (A) Coastal dunes Displacement (Cdn) over the mangroves and paleodunes (Pd), (B) Intertidal zone (Es) in the beach-barrier (Marco island), ridge and runnel (RR), High tide line (Htl) (C) beach-barrier in the Algodoal and Marco Islands; sand bars (Sb) in the Maracanã estuary, in the same direction of tidal currents; (D) Intertidal zone (Es), beach, mangrove and abrasion platform (Ap) on the Marco Island (photo from Guerreiro, 2010); (E) Abrasion platform (Ap) carved in the Barreiras Group sediments. The active cliffs (AF) indicate strong erosion in the Marco Island, in the back, the mangroves; (F) in the foreground the beach and ferruginous blocks, forming the abrasion platform (Ap) excavated in the Barreiras sediments (FB). In the background, the paleodunes (Pd) with a cross stratification tangential tabular in the Marco Island (photo from GUERREIRO, 2005).

4.1.1. Coastal Plateau

The Coastal Plateau (Fig. 1) is excavated in the Barreiras and Post-Barreiras sediments, constituting the regional geological base. This is presented in the form of flat surfaces, with straight, steep slopes, with heights up to 25 m. On the margins of the Maracanã Estuary, the Coastal Plateau appears in the form of active cliffs (Fig. 2F) and abrasion platforms (Fig. 2D, 2E, 2F), however, at the mouth it occurs in the form of active cliffs, abrasion platforms (Fig. 2D, 2E, 2F). These abrasion platforms are common and are formed in sandy and clayey sediments (Barreiras sediments), and parts in carbonate sediments (Pirabas Formation). This unit is located under active cliffs and exposed at low tide, forming discontinuous bands and variable extensions. Young mangroves often colonize abrasion platforms.

4.1.2. Coastal Plain

The MCP is based on recent clayey and sandy sediments (Fig. 1). This is the most significant unit, with flat topography and diverse geomorphological environments, close to sea level. It is cut by the Maracanã estuary and several tidal channels (Fig. 1). The following geomorphological units occur in the MCP: (i) muddy plain (mangroves), (ii) estuarine plain (estuary, tidal channels) and (iii) sandy plain (beaches, beach ridges, dunes, paleo-dunes, ebb tide pools, lakes).

Muddy Plain - The muddy plain is very extensive, developed on each side of the estuary and is the result of the effects of tidal variations. It is located between spring and mean tide levels (Fig. 1). Mangroves (Fig. 2A, 2D, 2E, 3D) take the form of almost horizontal lower terraces cut by tidal channels, and consist of fine sediments rich in organic matter. Tidal currents (ebb/flood) generate erosion, which gives rise to the development of mangrove terraces. However, it is common to observe progradational characteristics due to the colonization of young mangroves and the formation of muddy sandbanks at the mouth of tidal channels (Fig. 2C).

Estuarine Plain - The tidal plain is formed by channels, which are influenced by the tide and cut through the muddy plains, supplying sediment to the adjacent areas. These occur along the tidal flat, forming shoals and/or sinuous channels with variable widths, limited by mangroves and coastal plateau (Fig. 1). Point bars, channels through bars, islands and mangrove terraces can be observed. Examples of sandy structures (sand wave), mega-ripples occur in the back.

Sandy Plain - The sandy plain is located on the outer parts of the MCP (Algodoal and Marco Islands) (Fig. 3C), usually bordering mangrove, paleo dunes and coastal dunes, close to low tide level. It is represented by the inter tidal zone, where the sandy bars, beach cliffs, tidal channels occur, which flow into the infra tidal zone, in addition to the ebb tide delta. In this area, they are elongated tidal ridges, which follow the direction of tidal currents in the mouths of the major channels and Maracanã estuary.

In this plain, the beaches have a flat morphology and a slight slope towards the Atlantic Ocean, and occur in the northern and southeastern parts of the Algodoal and Marco islands (Fig. 2C). Occur obliquely to the coast, towards NW-SE. The arrow barrier beaches border the muddy plains (mangroves) and are cut by tidal channels (Fig. 3A). The macro tide and the gentle slope of the beaches influence the great extension (Fig. 2D). These 1 to 2 m high beach plain ridges are ancient shorelines, that is, they correspond to a system of old, continuous and discontinuous beach ridges that extend about 2 km east of Algodoal Island (Fig. 2C) and 1.5 km to the east part of Marco Island (Fig. 2C, 2D). The ebb tide delta, with flood/ebb channels, occurs at the mouth of the tidal channels, north of Algodoal Island. In these channels, mega-waves occur, parallel to the coast and perpendicular to the direction of the tidal flow. It is common to find paleo dunes (Fig. 2F) with layers up to 2 m thick and tabular and tangential stratification in the inner part of the coastal plain, sometimes limited between the mangroves and the coastal plateau, and sometimes at the base of the coastal dunes and in mangroves. Coastal dunes occur in the western and northern parts of the Algodoal Island, where they are sometimes associated with swamps at their edges, and in the northern part of the Marco Island. These dunes (Dcf) can be fixed by low-lying vegetation of vines and shrubs (Fig. 2A, 3B), preventing their migration. They are aligned in a NW/SE direction on the western side (Algodoal Island), with a maximum height of 10 to 12 m, where there are temporary lakes fed by rainwater (rainy season). The lakes are associated with dunes, paleodunes, coastal plains, and sometimes turn into muddy plains and coastal plateaus.

4.2. Vertical arrangement of sedimentological units

In the MCP, occur 6 sedimentological units: estuarine, point bar, dunes, mangrove, beach and sand bar deposits, and associated sediments: sand and mud, mud and sand, organic mud and sand, with different structures and mineral content, through which they can delimit the lateral and vertical correlations. Thus, it becomes possible, through side sections, three sedimentological units (S1, S2 and S3), which define depositional processes that occurred during the recent period.

4.2.1. Estuarine deposits

The estuarine deposits are composed of sand and mud (Fig. 4) and occur largely in the MCP, at a depth of 0.6 m. This deposit is superimposed on the mangroves and sandy beach deposits. This layer is interlaced, 20 to 120 cm thick with: (1) mud, the colour of which varies from dark grey (10YR 2/2), with a large amount of organic matter and plant debris, to greenish grey (10YR 2 /2) and (2) fine to very fine sand, interspersed with greenish grey mud, sometimes with organic matter, with flaser, linsen and and a plane-parallel stratification (Fig. 4). The particle size analysis revealed the presence of clay in the lower layer and a predominance of sand in the upper layer. The sediments were classified as sandy mud (bottom) and sandy mud (top), characteristic of moderate environmental hydrodynamics.

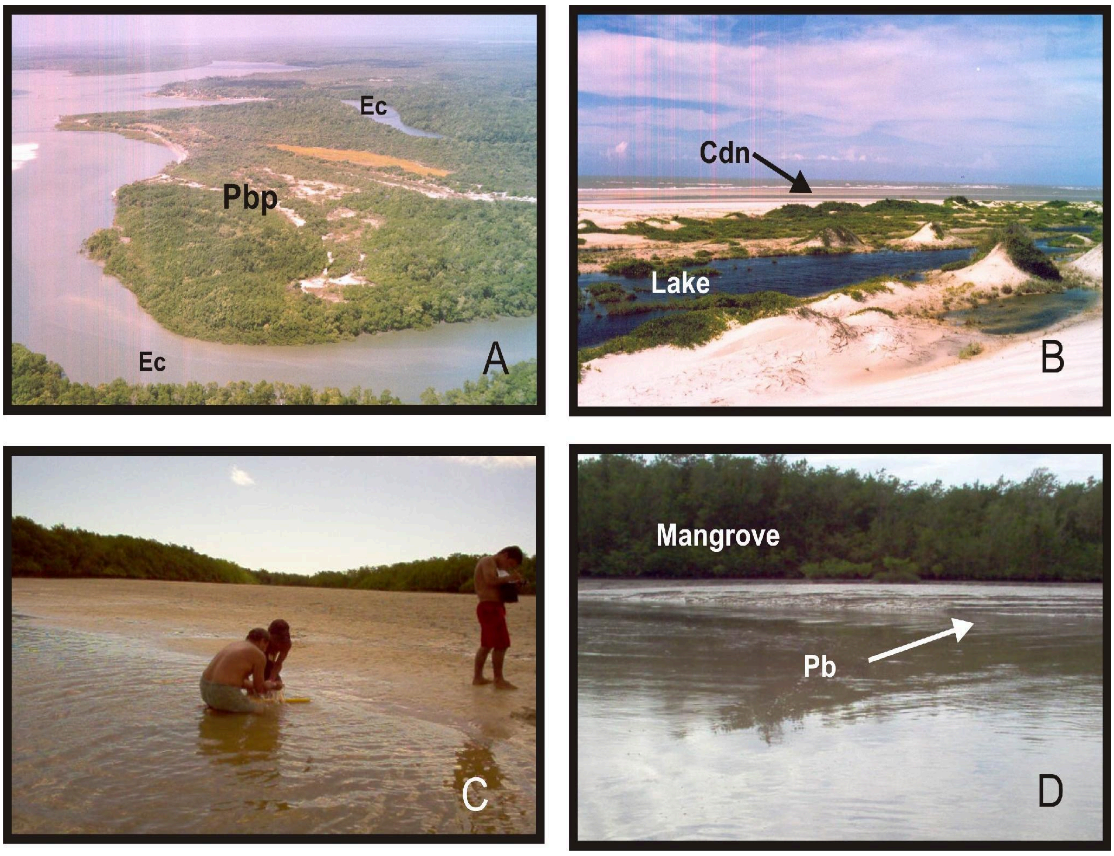

Figure 3: (A) Crest plain beach (Pbp), truncated by estuarine channel (Ec), (B) coastal dunes fields (Cdn) fixed by vegetation and note the presence of the lake, (C) sandy plain and the mangrove (background), (D) Point bar consisting of a sand and mud interleaving (Pb) on Cumarú Island.

4.2.2. Point bar deposits

Point bar deposits are located inside the floodplain and consist of interbedded thin layers of fine quartz sand and thick layers of mud with plant debris. While deposits located closer to the mouth of the tidal channels are sand bodies (with mud) (Fig. 4), most exposed, with heterolytic stratification. This unit reaches 3 m thick, with layers up to 25 cm of mud olive gray (5Y 6/1) and 5 cm of fine sand, whitish (5Y 8/1). Mud deposits with sand lamination's (beddings of flaser) (Fig. 4), typical bar in muddy spit, with a predominance of silt and clay fractions were observed. The silt prevails, particularly at the top of facies, while the lower part, the clay is more marked. The sands of this facies are thin to very thin, with a very homogeneous degree of selection. These sediments were classified as clay / sand (base) silt / clay at the top, characteristic of moderate environmental hydrodynamics.

4.2.3. Mangrove deposits

Mangrove deposits are flat, muddy layers more than 2 m thick, where, at the bottom, the mud contains a high concentration of organic matter and plant debris, ranging in color from gray to dark brown (10YR 2/2), with no defined structure (Fig. 4). However, at the top, there is silt (gray-brown in color-5YR 4/2) without plant debris, followed by a grayish-green layer (5YR 4/1) containing plant fragments.

Particle size is predominant clay at the top, but with a tendency to increase towards the bottom, silt predominating. These sediments are classified as clayey silt deposited under conditions of low to moderate hydrodynamics. Thus, sediments are deposited during the decrease of tidal currents during low tide, causing the deposition of fine sediments (mud and very fine sand).

4.2.4. Dune deposits

The dune deposits are represented by large dune fields (2-5 m high) with an EW direction and now overlap the beach deposits (Fig. 4), or over the mangroves. These dunes are made up of quartzose sands of fine to very fine grain, well selected, with fragments of shells and mica and grayish white (N8) and sometimes grayish yellow (5Y 8/1). The dunes are formed from the marine sand that arrives at the coast beach by waves. These dunes are made up of fine to very fine-grained quartz sands, well sorted, with fragments of shells and mica and grayish white (N8) and sometimes grayish yellow (5Y 8/1). They have tangential cross-stratification structures and are fixed by the vegetation, which often gives them stability, preventing migration.

4.2.5. Beach deposits

They consist of fine sand and medium-sized deposits from modern and ancient beaches (ridge beach plains).

Beach - They occur above the mangroves (infra tidal zone) (Fig. 4), with a thickness of 0.7 m, and low-angle stratification, generated from the migration of small ripples. It consists of a pack of light olive-green sand (5Y 4/1), corresponding to the sands of the beach plains, with a yellowish gray color (5Y 7/2), characteristic of current beaches. It is superimposed on the beach crest plain units and coastal dunes, or in direct contact with the Barreiras sediments. They are predominantly very fine sandy deposits (> 90%), with subordinate amounts of silt and clay (< 10%). At the top of the sedimentary column, the sands are well sorted, while at the bottom they are very well sorted, with negative to asymmetric asymmetry. The sediments were classified as sand, silt sand and clayey sand, submitted to a moderate hydrodynamic regime.

Crest beach plain (thickness of 1 m) - They are greenish gray sediments (5Y 6/1) at the top to a distressing pinkish gray color (5YR 8/1), with plane-parallel lamination's and low-angle inclinations, with wave bedding. The predominant particle size is represented by fine to very fine sand, very well selected and almost asymmetric. The clay and silt content reaches 15% and 10% respectively. This facies presents descending granocrescence, following the tendency of the distribution of silt and clay amounts.

4.2.6. Sand bars deposits

The sand bars are perpendicular to the coast and parallel to the tidal currents at the mouth of the Maracanã estuary and the tidal channels. These sand deposits show a progradational succession with upward clearance (upward thickening). Fine sediments to very fine deposition are mainly controlled by tidal currents, which are continually reworked and absorb a large part of the muddy sediments, through the re suspension process. These deposits are layers 2 m of yellowish gray sandy sediments (5Y 8/1), with thin lenses of mud (Fig. 4).

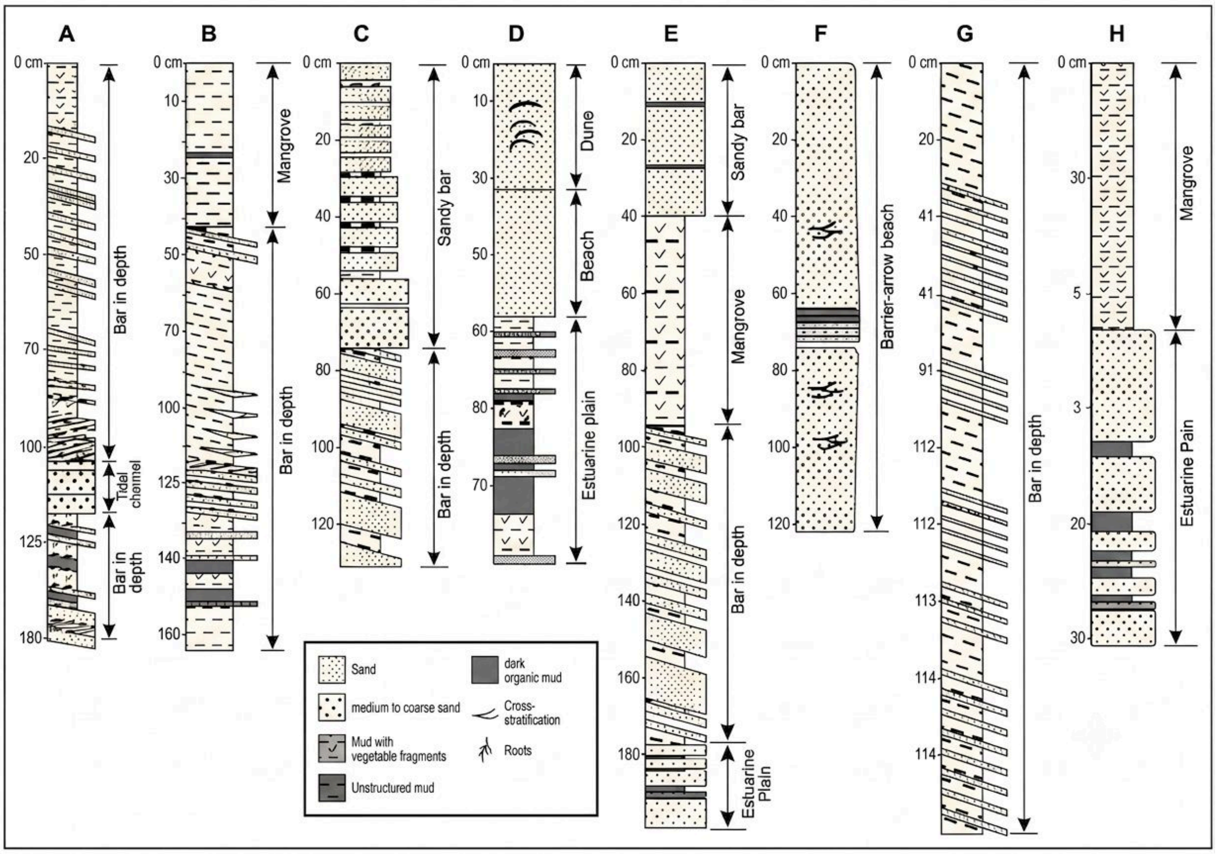

Figure 4: Profiles of the main sedimentological units in the MCP: (A) Bar in depth interspersed with sediments of tidal channel, (B) superimposed on mangrove sediments interleaved bar in depth, (C) sandy/clay and up bar in depth, (D) plain and estuarine sediments above sandy beach and dune, (E) Plain underposed estuarine sediments bar in depth, mangrove and sandy bar, (F) Beach, (G) mud with intercalation of sand blades (point bar) (H) Sand interspersed with layers of mud (estuarine plain) placed beneath the mangroves.

4.3. Sedimentological Units

Three sedimentary units were identified from the base to the top . The identification of lithofacies allowed the individualization of three sedimentary successions: Unit S1 occurs 2-3 m from the base. Each unit is a combination of features typical of a specific position in the depositional environment (Fig. 5). The following clay minerals were found: kaolinite, smectite and illite (main). The analysis of heavy minerals was limited to the sandy layers. Thus, 8 types of heavy minerals were identified in the MCP sediments: kyanite, staurolite, zircon, tourmaline, rutile, sillimanite, hornblende and epidote. The computed Zircon-Tourmaline-Rutile (ZTR index), indicating mineralogical maturity (Adamu et al. 2020, Hubert, 1962), showed that the most unstable ones (hornblende) are restricted to the sand layers of the point bar. On the other hand, the more stable (mature). minerals, such as zircon, rutile and tourmaline, occur more frequently, mainly in the sandy fraction.

4.3.1. S1 Unit

In Unit S1, marine/estuarine sand and mud facies (0.6 m thick) occur in most of the area. It is formed by an intercalation of beds of varying thicknesses (0.5 to 25 cm): (i) mud varies between dark gray (10YR 2/2), with a large amount of organic matter and plant debris, and greenish gray (10YR 2/2) (Fig. 5) and (ii) fine and very fine sands are intercalated with greenish gray mud, sometimes with organic matter, and bedding, sometimes flaser, sometimes linsen, with a flat-parallel layered structure. The sediments that make up this facies were classified as silty sand (upper) and silty-sandy sand (lower). In this sequence, the amount of smectite, with a percentage of 40% (minimum) and 49% (maximum), decreases towards the central part and then increases towards the lower part. The behavior of kaolinite is opposite to that of smectite, i.e. the amount increases (38%) towards the middle and then decreases (30%) towards the base. Illite remains constant (20%) (Fig. 6). The mineral composition reveals a limited presence of heavy minerals, in which zircon is the most abundant (56-35%), followed by staurolite (19-37%), rutile (8-12%), and tourmaline (9%), showing that the sediments are relatively mature (Fig. 7).

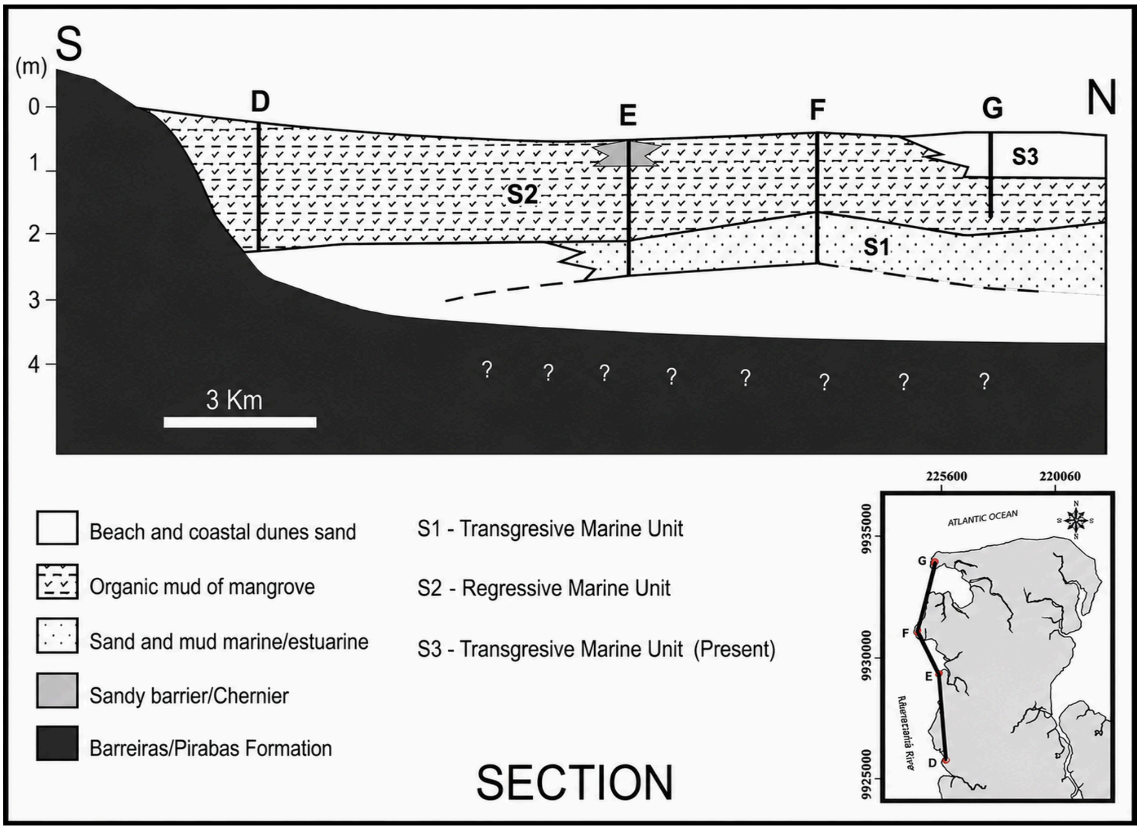

Figure 5: Section showing the S1, S2 and S3 sedimentological units on the right edge of the Maracanã Estuary. Below sedimentological units S1 and S2, there is no information.

4.3.2. S2 Unit

Unit 2 consists of: (i) silty clay, consisting of muddy deposits, brownish gray in color (5YR 4/2) and immediately followed by a greenish gray layer (5Y 4/1), with fragments of plant remains. At the base, the mud has a high concentration of organic matter and plant remains, with a dark brownish-gray color (10RY 2/2). The predominant grain size is clay (in the upper part) and silt (lower part) and (ii) muddier bars (inner part of the tidal plain) and sandier bars (outer part, near the mouth of the tidal channels). There are intercalations of sand (flaser-type beds) (5 cm of fine, whitish sand - 5Y 8/1) and mud (levels of up to 25 cm of olive gray mud - 5Y 6/1). In the organic mud facies (Fig. 1, 6B), clay minerals exhibit homogeneous behavior, with smectite being the most abundant, varying between 39% and 42%; kaolinite between 30% and 32%; and illite being less representative, with a constant value of 28%. In contrast, the behavior of clay minerals in the organic mud facies is relatively different, showing that smectite varies from 42% to

47%, kaolinite from 33% to 37%, and illite reaches values from 15% to 24% (Figs. 1, 6). In this case, the highest illite values are in the upper part of the facies, showing an inverse relationship with the other clay minerals. On Cumaru Island, the most representative minerals in the basic-medium direction of core B (Fig. 1, 6B) (sand and mud with point bars) are staurolite (31-40%), zircon (22-26%), kyanite (11-9%), and epidote (10-4%). These values are found in cores B and D (Figs. 1, 7).

4.3.3. S3 Unit

S3 Unit occurs over mangroves. It is formed by very fine sand (> 90%) and silt/clay (< 10%) from beach plain ridges, light olive gray in color (5Y 4/1) and yellowish gray (5Y 7/2). It overlaps beach ridge plain and coastal dune units, or is in direct contact with sediments from Barreiras. It exhibits low-angle stratification.

The only detailed analysis of the behavior of clay minerals in these facies revealed values similar to those already found, with 44% smectite, 36% kaolinite, and 20% illite (Fig. 6). The sandy facies that make up this sequence are dominated by staurolite, zircon, kyanite, and epidote. In the upper part, zircon is the most representative mineral, with 33%, followed by staurolite with 29% and epidote with 9% (Fig. 7). In the middle part, the main minerals are staurolite, with 34%, zircon, with 19%, and epidote, with 16%. The lower part showed similar behavior to the previous one, where staurolite predominated with 31%, followed by zircon with 23% and epidote with 12% (Fig. 7). A slight increase in minerals towards the top of the unit was observed.

5. Discussion

4.1. Sedimentary environments

The sedimentation (2 m thick) in the MCP indicates that the environments in bottom-up order (mangroves, dunes, beaches, sand and mud banks, delta tide, cheniers) were formed in the estuarine system, which shows that there were no changes substantial in the present. During the Late Holocene, through shoreline progradation (Behling et al. 2001, França et al. 2013, Dias et al. 2013, Cohen et al. 2021), this sedimentation was compartmentalized into three distinct situations S1, S2 and S3), according to the changing conditions of the sea level. The Average Dynamic Topography is up to 11 cm higher at the mouth of the Amazon River, with the Amazon flow having a local contribution to the mean sea level in this region. (Giffard et al. 2019). In the MCP, due to coastal areas represent complex environmental systems, as a high number of interacting variables (forcing factors, processes) control them, acting over different time scales (Aucelli et al. 2018). Due to the same authors, coastal landforms and sedimentary bodies, and their dynamics, are the result of the interaction between geological factors, neotectonic evolution and surface processes on a local scale, controlling sea level.

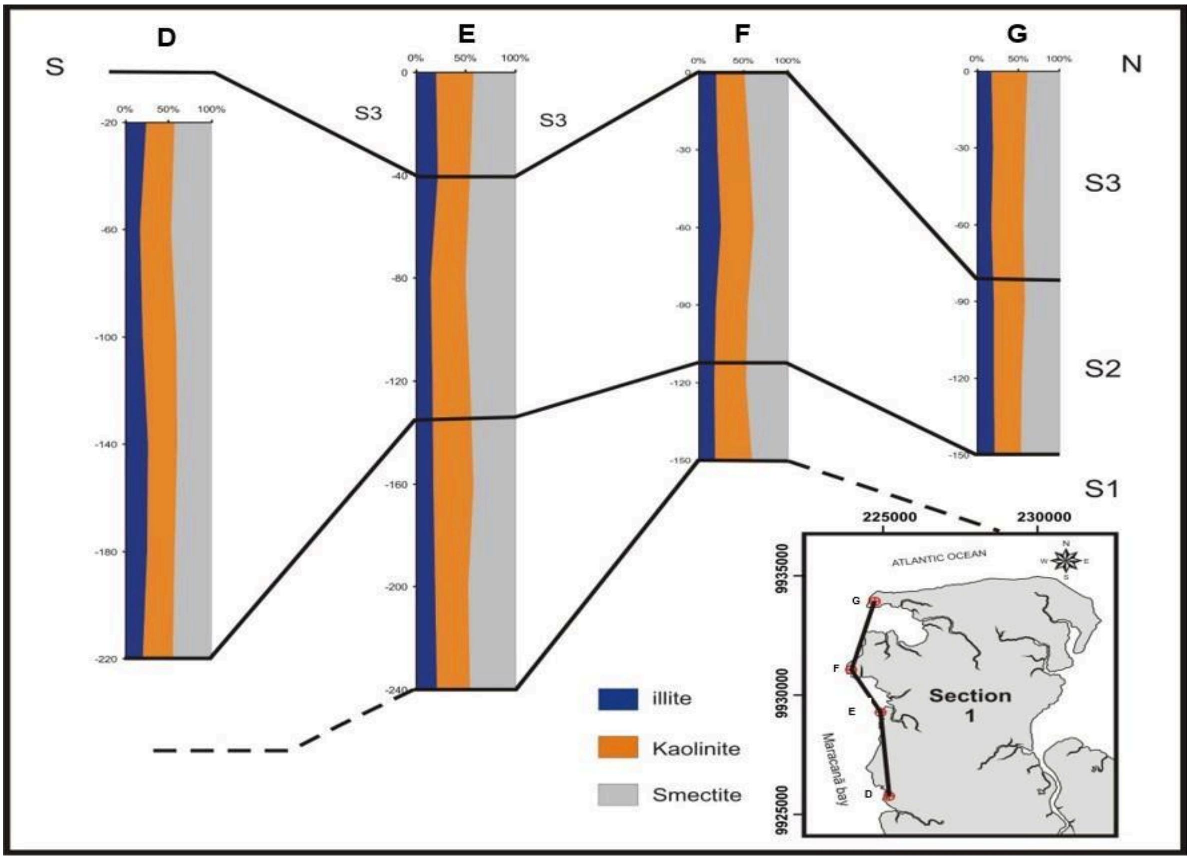

Figure 6: Vertical distribution of clay minerals in the S1, S2 and S3 sedimentological units on the right margin of the Maracana Estuary.

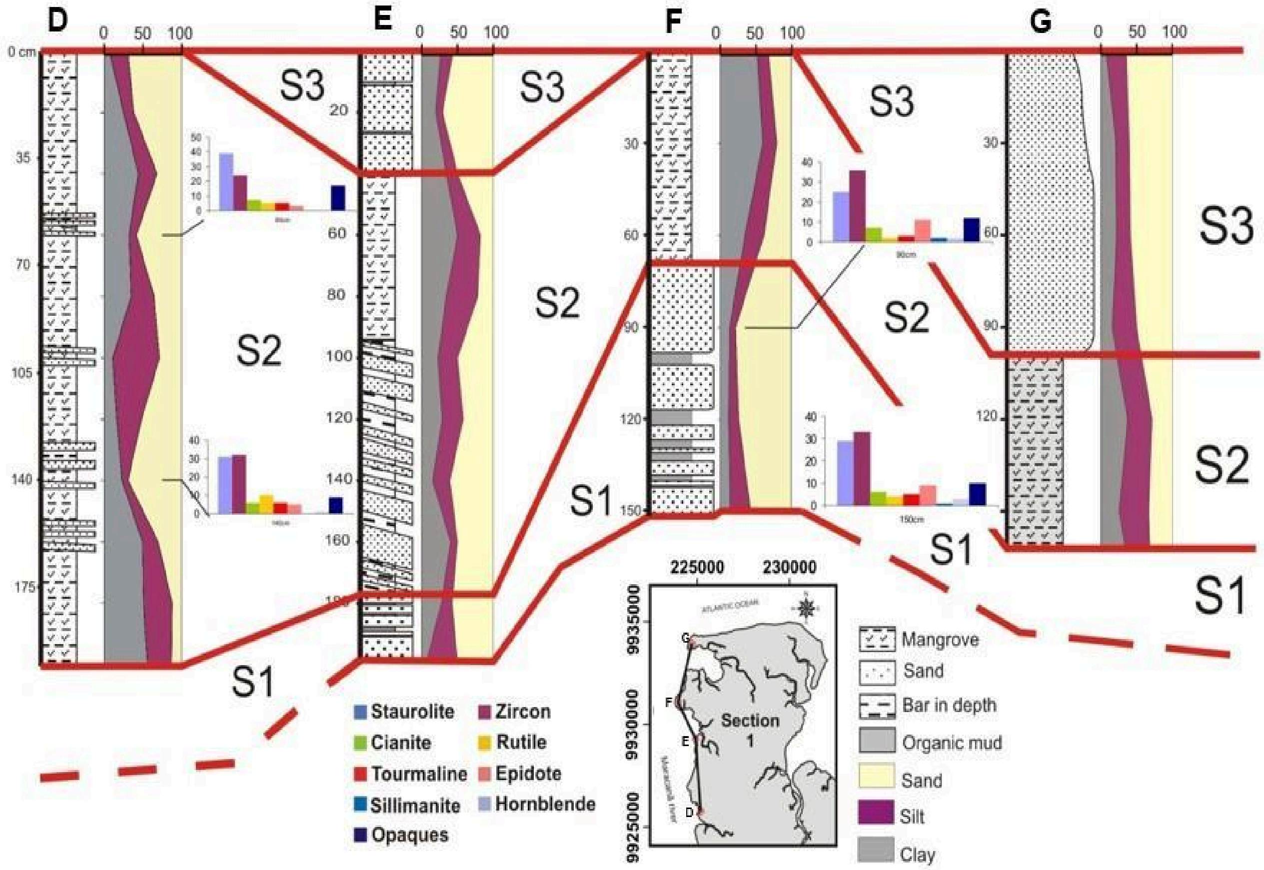

Figure 7: Vertical distribution of heavy minerals and grading percentage of sand, silt and clay, in the S1, S2 and S3 sedimentological units on the right board of the on the right margin of the Maracana Estuary.

5.2. I, II and III Units

Units S1 occurs at the base and consists of marine and estuarine mud and sand (Fig. 5). This marks the level of transgressive marine deposition, where the sediments are predominantly of sandy marine origin, interbedded with dark estuarine mud. These sediments were deposited under moderate hydrodynamic conditions. Unit 2 corresponds to a package of organic muddy sediments (mangrove), representing coastal zone accretion and deposited during the sea-level regression (Fig. 5). These sediments were possibly deposited under relatively stable marine conditions on vast plains, with little water agitation. S3 is a unit formed by sedimentary packages under the influence of tidal currents, waves, and winds (Fig. 5).

It is possible to observe the beach-to-dune system encroaching on the mangroves, indicating signs of beach retreat along the banks of the Maracanã estuary (Fig. 3B) and at the beach ridge bar (Figs. 3A, 3C), which implies coastal dynamics and recent SL events. The MCP is influenced by the effects of modern sea level rise (IPCC, 2022).

5.3. Heavy mineral and Provenance

The main heavy minerals were identified: staurolite, sillimanite, zircon, rutile, tourmaline and kyanite (Fig. 7). The kyanite, epidote, hornblende and sillimanite minerals are of metamorphic origin, mainly gneiss, mica-schists and amphibolites. The zircon is a representative of ultrastable minerals, appears with great frequency, and is considered incidental to plutonic rocks, or with accessory minerals in sedimentary rocks. The tourmaline is an ultra-stable mineral (borosilicate of calcium-sodium-iron-magnesium-lithium), is common and is present in all strata, representing less than 10%. The rutile occurs as a common mineral, representing less than 10% of the mineralogical assembly. The epidote is typical of metamorphic and/or hydrothermal origin, may be the result of the change of plagioclase (hydrothermal), or also by the change in garnet, pyroxene and amphibole, and occurs in quartzite and limestone, as the alteration product. The presence of kyanite suggests that the immediate origin is likely related to the restructuring of the Barreiras Group and Post-Barreiras sediments, as these minerals are present in their mineralogical composition (Nascimento & Góes, 2005). The metastable minerals are represented by staurolite and kyanite, which may indicate metamorphic sources. In fact, investigations conducted on Barreiras Group sediments in the region reveal a set of heavy minerals (staurolite, zircon, rutile, kyanite, monazite, epidote, tourmaline) (Góes, 1981), practically similar to those identified in this article (staurolite, zircon, kyanite, epidote). Thus, it can be suggested that these sediments originate primarily from the Barreiras Group sediments, which occur along the entire Atlantic Coast of Pará and on the adjacent continental shelf (El Robrini et al. 2018a).

5.4. Clay Mineral Provenance

Clay minerals may be used as a good indicator of the source area, weathering intensity and maturity of both sedimentary rocks and modern marine and fluvial sediments (Guyot et al. 2005). The Andean mountainous environment controls the geochemistry of the Amazon River (Gibbs, 1967) and concluded that the Andes were the source of 82% of the total suspended solids exported by the Amazon River.

The importance of Andean sources of suspended sediment to the main-stem Amazon River was re-affirmed by Meade et al. (1985) and others, who concluded that between 90% and 95% of the suspended sediment load of the main stem derived from the Andean tributaries. Due to Guyot et al. (20057), clay mineral composition highlights the evolution of the Madeira and Marañón–Solimões River, which start in the Andes with high illite + chlorite content. Due to the same authors, all Amazon shield tributaries (Brazilian, Guiana) show high kaolinite content and the lower Amazon River is characterized by relatively high smectite content. As they flow across the Amazon floodplain, Andean rivers exhibit a marked enrichment in smectite, derived from lateral erosion of the banks, as suggested by Johnsson and Meade (1990), and/or from tributaries that drain large Miocene sedimentary sequences. The two Andean tributaries, Solimões and Madeira, together, are responsible for 80-95% of the sediment production that is carried to the Atlantic Ocean annually (Filizola Jr. & Guyot, 2009, Latrubesse et al. 2005, Meade et al. 1985), while only a small part is supplied by the cratonic tributaries of the Japurá, Negro, Trombetas, Tapajós and Xingu rivers (Meade et al. 1985, Gibbs, 1967, Viers et al. 2008). Authors indicate that 85-95% of the suspended material consists of silt and clay-sized particles (Meade et al. 1985, Gibbs, 1967). There is very strong evidence that although the net transport of water from the Amazon River was towards the NW, due to the North Coastal Current of Brazil, seasonal changes in wind direction result in the formation of a counter-current near the coast that transfers part of the plume along the Atlantic Coast of Pará (Diegues, 1973). This assertion was corroborated by Morozov et al. (2024), who confirm that in addition to the plume spreading to the NW (towards the Guianas), part of the Amazon River plume migrates eastward, towards the Atlantic Coast of Pará. This condition contributes to the transfer of clay minerals originating from the Andean Chain to the MCP.

The clay minerals identified in the sediments of 1, 2 and 3 Units were smectite, kaolinite and illite. The first two predominate in all units (Fig. 6). The dispersal routes of clay minerals from the source to the deposition site depend on fluvial transport. In the Amazon Region, the equatorial climate (Dubreuil et al. 2019), favors large inputs of fine sediments (clay minerals) to the coastal/estuarine zone. Kaolinite was identified in all cores and depths analyzed. Due to Guyot et al. (2005), illite and chlorite can mark young sediments and soils close to the source areas (mainly plutonic rocks), and smectites characterize poorly drained tropical soils. In contrast, kaolinite marks well-developed leached soils and mature sediments under a tropical climate and, more especially, high rainfall inducing intense weathering.

However, smectites can also characterize the intensity of intermediate weathering (Saleemi & Zulfiqar, 2000; Thiry, 2000). It can also be formed by the transformation of pre-existing minerals, such as smectite, common on the Atlantic Coastal of Pará. At the MCP, clay minerals (smectite, kaolinite and illite) exhibit almost the same rates in I, II and III Units. The illite and chlorite of the Andean domain are products of the mechanical erosion of the plutonic and metamorphic rocks of the Cordillera. The basic rocks favored the formation of chlorite (ferromagnesium) instead of illite (potassium). The latter seem more representative in assemblages derived from acid petrographic provinces (Parra et al. 2009). Kaolinite and smectite from depressed regions under hot and humid tropical climate provide respectively laterite and neoformation hydrolysis in poorly drained coastal plains.

6. Conclusions

There are no similar studies in this section of the Coastal Plateau that extends into the Atlantic Ocean, where narrow, incised coastal plains are embedded within the plateau, occurring along the margins of numerous estuaries, such as the MCP. At the surface, the study revealed several geomorphological units in the MCP: (i) mudflat (mangroves), (ii) estuarine plain (estuary, tidal channels), and (iii) sandy plain (beaches, coastal bars, dunes, paleodunes, ebb tide pools, lakes). However, in the MCP sub-bottom, three sedimentary units were identified from the base to the top: (i) S1 resting on the Barreiras Group sediments (silt/sand—upper and sand/silt—lower), with a predominance of smectite and zircon; (ii) S2 (silty clay with intercalations of fine sand and mud, with a predominance of smectite and staurolite); (iii) S3 (very fine sands), with a predominance of smectite and staurolite. These results support an Andean source, where the clay minerals indicate an abundance of smectite; however, the presence of heavy minerals, such as zircon and staurolite, in the three sedimentary units indicates the immediate source of the Barreiras Group and Post-Barreiras sediments (present throughout the Atlantic Coast of Pará), which contain these minerals in their mineralogical composition. Sea level rise plays an important role in the evolution of the coastal and estuarine zone. In this case, the submergence of the coastal plain and the erosion of the coastal plateau produced changes in the arrangement of the coastal depositional systems. It is suggested that the study be repeated in other estuaries in the region.

Acknowledgement

Acknowledgment to the Ocean Geology Laboratory (LAGEOC) and the Marine and Coastal Studies Group (GEMC/CNPq at UFPA.

Credit author statement

M.E.R.: Conceptualization, Data curation, Formal analysis, Funding acquisition, Investigation, Methodology, Project administration, Validation, Visualization, Writing – original draft, Writing – review & editing.

References

ADAMU, L. M. OBAJE, N. G. OKAFOR, P. N. & UMAR, M. U. 2020. Integrated geochemical and multivariate statistical examination of source rocks in the Sokoto and Anambra Basins, Nigeria. Implications for Hydrocarbon Prospectivity, Petroleum Science and Engineering, 4(2), 39-50. https://doi.org/10.11648/j.pse.20200402.11.

ALBERS, A. P. F. MELCHIADES, F. G. MACHADO, R. BALDO, J. B. & BOSCHI, A. O. 2001. Um método simples de caracterização de argilominerais por difração de raio-x. Anais do 46º Cong. Bras. de Cerâmica. Florianópolis - SC. (46): 35-38.

AGÊNCIA NACIONAL DE ÁGUA E SANEAMENTO BÁSICO - ANA. Disponible in: https://www.gov.br/ana/pt-br. Acessed in: 04/11/2025.

ASSIREU, A. PIMENTA, J. SAAVEDRA, O. CAMACHO, R. EL ROBRINI, M. & PIMENTA, F. 2024. Favorable regions for hydrokinetic generation in the Maracanã estuary, Brazilian Amazon, from GPS-tracked drifters. Mediterranean Geosciences Union, 4TH Annual Meeting, Barcelona, Spain, 1-13.

AUCELLI, P. C. MATANO, F. SALVINI, R. & SCHIATTARELLA, M. 2018. Coastal changes, from past records to future trends: proxy analysis, modelling, and monitoring. Journal of Coastal Conservation, 22, 821-825. https://doi.org/10.1007/s11852-018-0623-z.

BAUM, M. P. KENNEDY, D. M. & MCSWEENEY, S. L. 2024. Large structural estuaries: Their global distribution and morphology, Geomorphology, 461, 1-11. https://doi.org/10.1016/j.geomorph.2024.109309.

BEHLING, H. COHEN, M. C. L. & LARA, L. 2001. Pollen analysis of modern mangrove systems. Palaeogeography, Palaeoclimatology, Palaeoecology, 167(3), 225-242. https://doi.org/10.1016/S0031-0182(00)00239-X.

BEZERRA, D. DA S. AMARAL, S. KAMPEL, M. & ANDRADE, P. R. DE. 2014. Simulating Sea-Level Rise Impacts on Mangrove Ecosystem adjacent to Anthropic Areas: the case of Maranhão Island, Brazilian Northeast. Pan-American Journal of Aquatic Sciences, 9(3), 188-198. Disponible in: https://api.semanticscholar.org/CorpusID:56292735.

BEZERRA, I. S. A. A. NOGUEIRA, A. C. R. GUIMARÃES, J. T. F. & TRUCKENBRODT, W. 2015. Late Pleistocene sea-level changes recorded in tidal and fluvial deposits from Itaubal Formation, onshore portion of the Foz do Amazonas Basin, Brazil. Brazilian Journal of Geology, 45(1), 63-78. https://doi.org/10.1590/2317-4889201530124.

BOYLES, J. M. SCOTT, A.J. & RINE, J. M. 1986. A logging form for graphic descriptions of core and outcrop. J. Sediment. Petrol. 56, 567-568.

BUSO, A. PESSENDA, L. C. R. OLIVEIRA, P. E. COHEN, M. C. L. GIANNINI, P. C. F. SCHIAVO, J. A. ROSSETTI, D. F. VOLKMER-RIBEIRO, C. & LORENTE, F. L. 2013a. Late Pleistocene and Holocene vegetation, climate dynamics, and amazonian taxa in the Atlantic rainforest of Linhares, Southeastern Brazil. Radiocarbon, 55, 1747-1762, 2013a. https://doi.org/10.1017/S0033822200048669.

BUSO, A. PESSENDA, L. R. OLIVEIRA, P. E. GIANNINI, P. C. F. COHEN, M. C. L. SCHIAVO, J. A. ROSSETTI, D. F. & VOLKMER-RIBEIRO, C. 2013b. From an estuary to a freshwater lake: a paleo-estuary evolution in the context of Holocene sea-level fluctuations, Southeastern Brazil. Radiocarbon, 55, 1735-1746. https://doi.org/10.1017/S0033822200048657.

CASTRO, J. W. A. SUGUIO, K. SEOANE, J. C. S. & DA CUNHA, A. M. 2014. Sea-level fluctuations and coastal evolution in the state of Rio de Janeiro, Southeastern Brazil. Annals of the Brazilian Academy of Sciences, 86(2), 1678-2690. https://doi.org/10.1590/0001-3765201420140007.

CAVALCANTE, G. H. FEARY, D. A. & KJERFVE, B. 2013. Effects of tidal range variability and local morphology on hydrodynamic behavior and salinity structure in the Caeté River Estuary, North Brazil. International Journal of Oceanography, 1-10. https://doi.org/10.1155/2013/315328.

COHEN, M. C. L. CAMARGO, P. M. P. PESSENDA, L. C. R. LORENTE, F. L. SOUZA, A. V. DE, CORRÊA, J. A. M. BENDASSOLLI, J. & DIETZ, M. 2021. Effects of the middle Holocene high sea-level stand and climate on Amazonian mangroves. Journal of Quaternary Science, 36 (6), 1013-1027. https://doi.org/10.1002/jqs.3343.

COHEN, M. C. L. FIGUEIREDO, B. L. & OLIVEIRA, N. N. 2020. Impacts of Holocene and modern sea-level changes on estuarine mangroves from northeastern Brazil. Earth Surface Processes and Landforms, 45, 375-392. https://doi.org/10.1002/esp.4737.

COSTA, J. B. S. BEMERGUY, R. L. HASUI, Y. BORGES, M. S. JUNIOR, C.R.P.F. BEZERRA, P. E. L. COSTA, M. L. & FERNANDES, J. M. G. 1996. Neotectônica da região Amazônica: aspectos tectônicos, geomorfológicos e deposicionais. Geonomos, 4 (2), 23-44.

DIRETORIA DE HIDROGRAFIA E NAVEGAÇÃO - DHN. 2026. Available from: www.dhn.mar.mil. Tidal data. consultation held on March 5.

DIAS, F. F. GUIMARÃES, J. T. F. COHEN, M. C. L. FRANÇA, M. C. PESSENDA, L. R. & BEHLING, H. 2013. Morphological and vegetation changes on tidal flats of the Amazon coast during the last 5000 cal. yr BP. Holocene, 23, 528-543. Available from: https://journals.sagepub.com/doi/abs/10.1177/0959683612463097.

DIÉGUES, F. M. F. 1973. Introdução à oceanografia do estuário Amazônico. In: Congresso Brasileiro de Geologia, Belém, v. 26 (2), 301-18.

DUBREUIL, V. FANTE, K. P. PLANCHON, O. & SANT'ANNA NETO, J. L. 2019. Climate change evidence in Brazil from Köppen's climate annual types frequency. J. Climatol, 39, 1446-1456. Available from: https://doi.org/10.1002/joc.5893.

DUNNE T. MERTES L. A. K. MEADE R. H. RICHEY, J.E. & FORSBERG, B.R. 1998. Exchanges of Sediment Transport Between the Floodplain and Channel of the Amazon River in Brazil. Geological Society of America Bulletin, 110(4): 450-467.

EL-ROBRINI, M. MAGNO, P.V. & RANIEIRI, L. A. GUERREIRO, J. S. 2024. Seasonal and macrotidal influence on the morphodynamics of estuarine beaches (Marajó island - Eastern amazon - Brazil). Quaternary and Environmental Geosciences, 15, 20-34. https://doi.org/10.5380/qeg.v15io.94228.

EL ROBRINI, M. 2012. Morfologia e sedimentação de fundo na baía do Marajó e na plataforma continental interna rasa: influenciadas por macro-maré. In Book: Oceanografia, Meio Ambiente e Governança Ambiental, 177-188. Available from: ISBN 978-85-913261-0-5.

EL ROBRINI, M. & BARBOSA, L. P. F. 2012. Forçantes oceanográficas na foz do estuário do rio Pará (baía do Marajó)(Amazonia Oriental). In Book: A foz do rio Pará (Amazonia Oriental) Oceanografia, Meio Ambiente e Governança Ambiental, 71-104. Available from: ISBN 978-85-913261-0-5.

EL-ROBRINI, M. RANIERI, A. L. SILVA, P. V. M. GUERREIRO, J. S. ALVES, M. A. M. S. DA, OLIVEIRA, DE R. R. S. SILVA, M. D. O. S. F. DA, AMORA, P. B. C. EL ROBRINI, M. H. S. & FENZL, N. 2018a. Erosão e Progradação da zona costeira e Estuarina do Pará. In: Panorama da Erosão Costeira no Brasil. Ministry of the Environment Brazil, 60-161. Available from: ISBN: 978-85-7738-394-8.

EL-ROBRINI, M.. Santos, J. H. S. Dos, Lima, L. G. De, Santos, A. L. S. Dos. Santos, M. C. S. F. V. Dos & Souza, U. D. V. 2018b.

Erosão e Progradação da zona costeira e Estuarina do Maranhão. In: Panorama da Erosão Costeira no Brasil. Ministry of the Environment Brazil, 66-167. Available from: ISBN: 978-85-7738-394-8.
FAGUNDES, H. FLEISCHMANN, A. FAN, F. PAIVA, R. BUARQUE, D. SIQUEIRA, V. COLLISCHONN, W. & BORRELLI, P. 2023. Human-Induced changes in South American river sediment fluxes from 1984 to 2019. Water Resources Research, 59 (6), 1-24. https://doi.org/10.1029/2023WR034519.
FIGUEIREDO JR. A. G. 1990. Normas de controle de qualidade para processamento de testemunhos inconsolidados. Projeto sedimentos de talude, Contrato PETROBRÁS/UFF n. 3-570-794-0-90, 27p.
FILIZOLA N. & GUYOT J. L. 2009. Suspended Sediment Yield in the Amazon Basin: an Assessment Using Brazilian National Data Set. Hydrological Processes, 23(22): 3207- 3215. https://doi.org/10.1002/Hyp.7394].
FRANÇA, M. C. ALVES, I. C. CASTRO, D. F. COHEN, M. C. L. ROSSETTI, D. F. PESSENDA, L. C. R. LORENTE, F. L. FONTES, N. A. BUSO, A. A. JR. GIANNINI, P. C. F. & FRANCISQUINI, M. I. 2015. A multi-proxy evidence for the transition from estuarine mangroves to deltaic freshwater marshes, Southeastern Brazil, due to climatic and sea-level changes during the late Holocene. Catena, 128, 155-166. https://doi.org/10.1016/j.catena.2015.02.005.
FRANÇA, M. C. COHEN, M. C. L. PESSENDA, L. R. ROSSETTI, D. F. LORENTE, F. L. BUSO, JR. A. A. GUIMARÃES, J. T. F. & FRIAES, Y. S. 2013. Mangrove vegetation changes on Holocene terraces of the Doce River, southeastern Brazil. Catena, 110, 59-69. https://doi.org/10.1016/j.catena.2015.02.005.
FRITZ, S. C. 2008. Deciphering climatic history from lake sediments. Journal of Paleolimnology, 39(1), 5-16. https://doi.org/10.1007/s10933-007-9134-x.
GAILLARDET, J. DUPRE, B. ALLEGRE, C.J. & NÉGREL, P. 1997. Chemical and physical denudation in the Amazon River Basin, Chemical Geology, 142 (3-4), 141-173. https://doi.org/10.1016/S0009-2541(97)00074-0.
GALEHOUSE, J. S. 1971. Point counting. In: Carver, R. E. ed. Procedures in Sedimentary Petrography. Wiley Interscience. New York, 385-407.
GERMANO, M. F. VITORINO, M. I. COHEN, J. C. P. COSTA, G. B. SOUTO, J. I. O. REBELO, M. T. C. SOUSA, A. M. L. 2017. Analysis of the breeze circulations in Eastern Amazon: an observational study. Atmospheric science letters, 18, 67-75. https://doi.org/10.1002/asl.726.
GIFFARD, P. LLOVEL, W. JOUANNO, J. MORVAN, G. & DECHARME, B. 2019. Contribution of the Amazon River Discharge to Regional Sea Level in the Tropical Atlantic Ocean. Water, 11, 1-16. https://doi.org/10.3390/w11112348. GUERREIRO, J. EL-ROBRINI, M. & RANIERI, L.A. 2013. Seasonal changes of a dynamic macrotidal beach: Case study of Marieta Beach (Amazon Coast/Brazil). Journal of Coastal Research, 65, 1780-1784. https://doi.org/10.2112/SI65-301.1.
GUERREIRO, J. S. FREIRE, A. P. DE & EL-ROBRINI, M. 2016. Cross-Shore sediment transport during an extreme event on Amazon Coast. Journal of Coastal Research, 2, 90-98. Available from: ISSN: 07490208.
GUERREIRO, J. S. SOUZA, E. B DE & EL-ROBRINI, M. 2020. Variability of Wave Spectra Conditions in the Amazon Barrier Coast. Journal of Coastal Research, I (95), 1411-1415. https://doi.org/10.2112/SI95-273.1.
GUYOT J. L. FILIZOLA N. & LARAQUE A. 2005. Régime et bilan du flux sédimentaire de l'Amazone à Óbidos (Pará, Brésil) de 1995 à 2003. In: Walling D.E. & Horowitz A.J. (eds.) Sediment Budgets 1. Osfordshire, IAHS, 347-354.
GIBBS, R. J. 1967. The geochemistry of the Amazon River system; part. I. The factors that control the salinity and the composition and concentration of the suspended solids. Geol Soc Am Bull, 78, 1203-1232.
GUIMARÃES, J. T. F. COHEN, M. C. L. FRANÇA, M. C. ALVES, I. C. C. SMITH, C. B. PESSENDA, L. C. R. & BEHLING, H. 2013a. An integrated approach to relate Holocene climatic, hydrological, morphological and vegetation changes in the southeastern Amazon region. Vegetation History and Archaeobotany, 22, 185-198. https://doi.org/10.1007/s00334-012-0374-y.
GUIMARÃES, J. T. F. COHEN, M. C. L. FRANÇA, M. C. PESSENDA, L. C. R. SOUZA, DE J. E. NOGUEIRA, A. C. R. & ALVES, R. 2013b. Recent effects of tidal and hydro-meteorological changes on coastal plains near the mouth of the Amazon River. Earth Surface Processes and Landforms, 38, 1535-1549. https://doi.org/110.1002/esp.3396.
GUYOT, J. L. JOUANNEAU, J. M. SOARES, L. BOAVENTURA, G. MAILLET, N. & LAGANE, C. 2007. Clay mineral composition of river sediments in the Amazon Basin. Catena, 71, 340-356. https://doi.org/10.1016/j.catena.2007.02.002.
GÓES, A. M. 1981. Estudo sedimentológico dos sedimentos Barreiras, Ipixuna e Itapecuru no nordeste do Pará e noroeste do Maranhão. 55 f. Dissertação (Mestrado) - Universidade Federal do Pará, Centro de Geociências, Belém, 1981. Curso de Pós-Graduação em Ciências Geofísicas e Geológicas.
HERBERT JR. & EL ROBRINI, M. 2024. Dinâmica Espaço-Temporal (1986-2020) de Manguezais de Resex da Foz do Rio Pará (Amazônia Oriental, BrasiL). Novos Cadernos NAEA, 27 (2), 301-323. ISSN 1516-6481/2179-7536.
HUBERT, J.F. 1962. A zircon-tourmaline-rutile maturity index and the interdependence of the composition of heavy mineral assemblages with the gross composition and texture of sandstones. Journal of Sedimentary Research, 32(3), 440-450. https://doi.org/10.1306/74D70CE5-2B21-11D7-8648000102C1865D.
HUMPHRIES, M. S. 2021. Elemental proxy evidence for late Quaternary palaeoenvironmental change in southern African sedimentary records: interpretation and applications. South African Journal of Geology, 124 (4), 1033-1046. https://doi.org/10.25131/sajg.124.0046.
HOCH, J. 2014. PCR-GLOBSET - Development and verification of a global sediment supply model. Master's thesis, University of Twente.
INSTITUTO NACIONAL DE METEOROLOGIA - INMET. 2025. Meteorological data. Available from: www.inmet.gov.br. Consultation held on December 3, 2025.
INTERGOVERNMENTAL PANEL ON CLIMATE CHANGE - IPCC. 2022. Climate Change 2022: Impacts, Adaptation and Vulnerability. Working Group II contribution to the Sixth Assessment Report, 166p. Available from: ISBN 978-92-9169-162-3.
JOHNSSON, M.F. MEADE R.H. 1990.
Chemical weathering of fluvial sediments during alluvial storage: The Macupanin Island point bar, Solimo˜es River, Brazil
Journal of Sedimentary Petrology, 60, 827-842.
LATRUBESSE, E.M.. STEVAUX, J.C. & SINHA. R. 2005. Tropical Rivers. Geomorphology 70, 187-206.
MARTINEZ, J. M. GUYOT, J. L. FILIZOLA, N. & SONDAG, F. 2009. Increase in suspended sediment discharge of the Amazon River assessed by monitoring network and satellite data, CATENA, 79 (3), 257-264. https://doi.org/10.1016/j.catena.2009.05.011.
MASCARENHAS, A. C. C. 2024. Contribuição continental hídrica e de nutrientes do sistema de reentrâncias, Norte do Brasil, Tese de Doutorado. Programa de Pós-Graduação em Geofísica, UFPA, 91p.
MAURICE-BOURGOIN, L. BONNET, M. P. MARTINEZ, J. M. KOSUTH, P. COCHONNEAU, G. MOREIRA. TURCQ, P. GUYOT, J. L. VAUCHEL, P. FILIZOLA, N. SEYLER, P. 2007. Temporal dynamics of water and sediment exchanges between the Curuai floodplain and the Amazon River. Brazil. J. Hydrol. 335, 140-156.
MAY, S. M. PINT, A. RIXHON, G. KELLETAT, D. WENNRICH, V. & BRÜCKNER, H. 2013. Holocene coastal stratigraphy, coastal c changes and potential palaeoseismological implications inferred from geo-archives in Central Chile (29-32° S). Zeitschrift für Geomorphologie, 57 (4), 201-228. https://doi.org/10.1127/0372-8854/2013/S-00154.
MEADE, R. H. DUNNE, T. RICHEY, J. E. SANTOS, U. DE. M. & SALATI, E. 1985. Storage and remobilization of suspended sediment in the lower Amazon River of Brazil. Science, 228, 488-490. https://doi.org/10.1126/science.228.4698.488.
MENEZES, R. A. A. GUIMARÃES, D. K. M. & El ROBRINI, M. 2024. Variations of the Coastline in a Medium Period

(1985-2017) of a tropical Island: the Case of Soure (Marajó - Pará/BRAZIL). Boletim Paulista de Geografia, 112, 51-76. ISSN: 2447-0945.

MIRANDA, L. B. DE, MENDES, B. & KJERFVE, B. 2012. Principios de Oceanografia Fisica de Estuários. Editora da USP, 414p. Available from: ISBN: 9788531406751.

MOLINIER, M. GUYOT, J. L. OLIVEIRA, E. D. & GUIMARAES, V. 1996. Les régimes hydrologiques de l'Amazone et de ses affluents. Hydrologie Tropicale: Géoscience et Outil Pour le Développement. IAHS publication 238, 209-222I.

MOROZOV, E. G. FREY, D. I. SALYUK, P. A. & BUDYANSKY, M. V. 2024. Amazon River Plume in the Western Tropical North Atlantic. J. Mar. Sci. Eng. 12, 851, 1-18. https://doi.org/10.3390/jmse12060851.

NASCIMENTO, M. S. & GÓES, A. M. 2005. Distribuição estratigráfica e proveniência de minerais pesados das Formações Ipixuna e Barreiras, região do Rio Capim, sul da sub-bacia de Cametá. Revista Brasileira de Geociências, 35 (1), 49-58. https://doi.org/10.25249/0375-7536.20053514958.

OLTMAN, R. R. 1968. Reconnaissance Investigations of the Discharge and Water Quality of the Amazon River. Geologica Survy, circular 522, 1-22.

PARRA, M. MORA, A. SOBEL, E. R. STRECKER, M. R. & GONZÁLEZ, R. 2009. Episodic Orogenic Front Migration in the Northern Andes: Constraints from Low-Temperature Thermochronology in the Eastern Cordillera, Colombia. Tectonics, 28, 1-27. https://doi.org/1010.1029/2008TC002423.

PELLETIER, J. 2012. A spatially distributed model for the long-term suspended sediment discharge and delivery ratio of drainage basins. Journal of Geophysical Research (Earth Surface), 117, 2028.

RANIERI, L. A. & EL-ROBRINI, M. 2015. Evolução da linha de costa de Salinópolis, Nordeste do Pará, Brasil. Pesquisas em Geociências, 42 (3), 207-226. https://doi.org/10.22456/1807-9806.78121.

RANIERI, L. A. & EL-ROBRINI, M. 2016. Quantificação de sedimentos transportados por correntes nas praias oceânicas de Salinópolis, nordeste do Pará, Brasil. Geociências, 35 (3), 457-471. Available from: ISSN 0101-9082.

RANIERI, L. A. ROSARIO, R. P. TRITINGER, A. S. & EL-ROBRINI, M. 2022. Coastal dynamics on equatorial beaches of Amazonian coast during extreme tide events. Pesquisas em Geociências , 41, 1-16. https://doi.org//10.22456/1807-9806.116073.

RANIERI, L. A. & EL-ROBRINI, M. 2020. Morfologia e sedimentação em praias oceânicas da Amazônia Oriental durante a variação anual de chuvas. Revista Brasileira de Geografia Física, 13, 2086-2102. https://doi.org/10.26848/rbgf.v13.5.p2086-2102.

RÖBER, B. & RUDOLPHI, H. 2004: Impacts of sea level changes on coastal regions – a local study for SEAREG. Coastline Reports 2, SCHERNEWSKI, G. & LÖSER, N. (eds.): Managing the Baltic Sea, 185-194. Available from: SSN 0928-2734.

ROSSETTI, D. DE. F. ROCCA, R. R. & TATUMI, S. H. 2013. Evolução dos sedimentos Pós-Barreiras na zona costeira da bacia São Luís, Maranhão, Brasil. Bol. Mus. Para. Emílio Goeldi. Cienc. Nat. 8 (1), 11-25. https://doi.org/10.46357/bcnaturais.v8i1.578.

SALEEMI, A. A. & ZULFIQAR, A. 2000. Mineral and chemical composition of Karak Mudstone, Kohat Plateau, Pakistan: implications for smectite-illitization and provenance. Sedimentary Geology, 130, 229-247. https://doi.org/10.1016/S0037-0738(99)00113-X.

SAWCZYŃSKI, S. & KACZMAREK, L.M. 2014. Sediment transport in the coastal zone. Technical Sciences, 17(2), 165-180. Available from: ISSN 1505-4675

SILVA, P. V. M. & EL ROBRINI, M. 2025. Influence of the macrotide on the beaches of Algodoal Island (Paraense Atlantic Coast -Eastern Amazon/ Brazil). Pesquisas em Geociencias, 52 (2), 1-18. https://doi.org/10.22456/1807-9806.140788.

SOUZA, L. S. B. ROSSETTI, D. DE. F. & PRADO, R. L. 2014. Radar de penetração no solo aplicado à caracterização de estruturas tectônicas miocênicas e quaternárias no leste da ilha do Marajó (PA). Brazilian Journal of Geology, 44(1), 55-72. https://doi.org/10.5327/Z2317-4889201400010006.

TANABE, S. NAKASHIMA, R. & MIZUNO, K. 2022. Holocene filling of a narrow estuary in a regressive coast: The Paleo-Kinu Bay region, central Japan. Marine Geology, 447, 1-16. https://doi.org/10.1016/j.margeo.2022.106795.

THE ROCK-COLOR CHART COMMITTEE. Munsell Geological Rock-Color Chart. Revised Washable Edition. Page Dimensions: 4-3/8" x 7-1/4". Binder Dimensions: 6" x 7-3/4" x 1", 2009.

THIRY, M. 2000. Palaeoclimatic interpretation of clay minerals in marine deposits: an outlook from the continental origin. Earth-Science Reviews, 49, 201-221. https://doi.org/10.1016/S0012-8252(99)00054-9.

VIERS, J. RODDAZ, M. FILIZOLA, N. GUYOT, J.L. SONDAG, F. BRUNET, P.; ZOUITEN, C. BOUCAYRAND, C. MARTIN, F. & BOAVENTURA, G. R. 2008. Seasonal and provenance controls on Nd–Sr isotopic compositions of Amazon rivers suspended sediments and implications for Nd and Sr fluxes exported to the Atlantic Ocean. Earth and Planet. Sci. Lett. 274 (3), 511-523. https://doi.org/10.1016/j.epsl.2008.08.011.

XIONG, D. ZHOU, H. & CHANGJIANG, D, U. 2006. A review on soil crack study. Soil, 38(3), 249-255. https://doi.org/10.36783/18069657rbcs20190169.

YU, D. LIU, S. LI, G. ZHONG, Y. LIANG, J. SHI, J. LIU, X. & WANG, X. 2022. The River–Sea Interaction off the Amazon Estuary. Remote Sens, 14 (4), 1-17. https://doi.org/10.3390/rs14041022.

ZHANG, Y. CHIESSI, C. M. MULITZA, S. ZABEL, M. TRINDADE, R. I. F. HOLLANDA, M. H. B. M. DANTAS, E. L. GOVIN, A. TIEDEMANN, R. & WEFER, G. 2015. Origin of increased terrigenous supply to the NE South American continental margin during Heinrich Stadial 1 and the Younger Dryas. Earth and Planetary Science Letters, 432, 493-500. https://doi.org/10.1016/j.epsl.2015.09.054.

[1]Recebido 11 de novembro de 2025
Aceito 03 de julho de 2026